Chapter 2

Model of Turbulent Magnetic Field

Since this research focus on the effect of turbulent magnetic fields in interplanetary space on the motion of solar energetic particles, in this chapter we present the model of magnetic field that we use. One is two-component magnetic turbulence to study the separation and another one is turbulent magnetic field with Taylor microscale to find the technique of measurement. We also assume that the magnetic field is static and homogeneous.

2.1 Two-Component Magnetic Turbulence

The two-component model was motivated by the observation that solar wind fluctuations are concentrated at nearly parallel and nearly perpendicular wave number (Matthaeus, Goldstein, & Roberts 1990). For the parallel component, the wave vector is parallel to the direction of the mean field and the fluctuation of the magnetic field in this component is perpendicular to both the parallel wave vector and the mean field. This is motivated by Alfv̈enic or slab like waves in the solar wind propagating along the mean field. We call this component the "slab" component. Another component, which is motivated by laboratory experiments, is called "two-dimensional (2D)" turbulence, which has a wave vector perpendicular to the mean magnetic field. The magnetic fluctuation in this component is also perpendicular to both the wave vector and the mean field. This component gives long correlation lengths in the direction of the mean field. The analysis of solar wind data by Matthaeus, Goldstein, & Roberts (1990) showed that the power spectrum of the solar wind turbulence is composed of these two components. Furthermore, the two-component model provides a good explanation of the parallel transport of SEPs (Bieber et al. 1994; Bieber, Wanner, & Matthaeus 1996; Dröge 2000), providing a solution to the long-standing discrepancy between theoretical and observed scattering mean free paths.

Two-component magnetic model can be generally written as

$$\vec{B}(x,y,z) = B_0\hat{z} + \vec{b}_{slab}(z) + \vec{b}_{2D}(x,y). \tag{2.1}$$

The total magnetic field consists of the uniform mean field ($B_0\hat{z}$) and the transverse fluctuations ($\vec{b}_{slab}$ and $\vec{b}_{2D}$) which are in the perpendicular direction to the mean field. For the fluctuations, the slab (one dimensional) fluctuation depends on the z coordinate while the two dimensional (2D) fluctuation depends on the x and y coordinates (Chuychai 2004). Next, we introduce the characteristic of each type of magnetic field that we use in this research.

2.1.1 Slab Fluctuation

From the definition of the slab field, the fluctuation depends only on z. Therefore, if we consider the slab fluctuation in the x-y plane at each z, $\vec{b}_{slab}$ is the same along that plane but different from the field on other planes as shown in Figure 2.1.

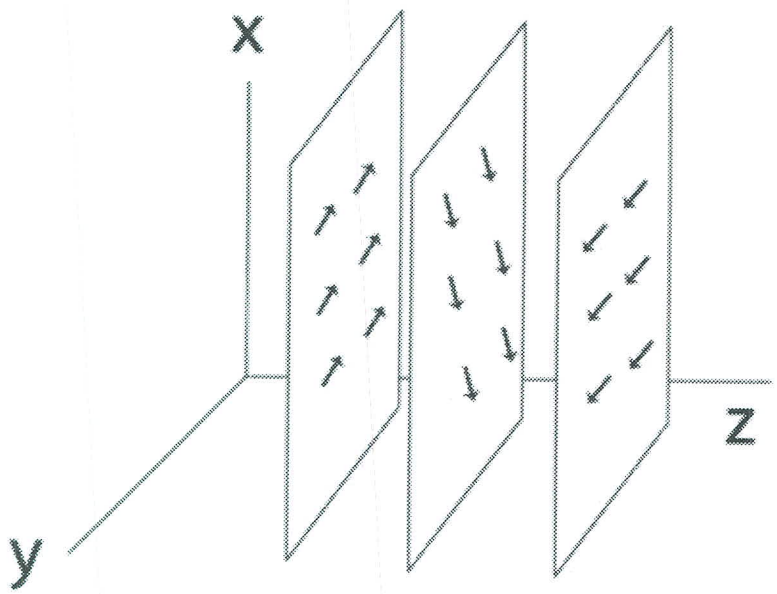

Figure 2.1 Illustration of the slab fluctuation, which depends only on the z coordinate. The arrows demonstrate the slab fluctuation $\vec{b}_{slab}$.

For the slab fluctuation, since the magnetic field is turbulent, the power spectrum is specified by a Kolmogorov spectrum, including an energy containing range and an inertial range with a 5/3 power law index, as

$$P_{xx}^{slab}(k_z) = P_{yy}^{slab}(k_z) = \frac{C}{[1+(k\lambda)^2]^{5/6}} \tag{2.2}$$

where λ is a coherence length and C is constant. See the shape of spectrum in Figure 2.2. To generate the slab magnetic field, we first numerically compute the field in Fourier space by using the power spectrum and a random phase, and then transform them back to real space via and inverse Fourier transform. Finally, we will have the magnetic field data over detailed grid in the simulation box. Figure 2.3 shows the example of trajectories of magnetic field lines from pure slab turbulence $[B_0\hat{z} + \vec{b}_{slab}(z)]$.

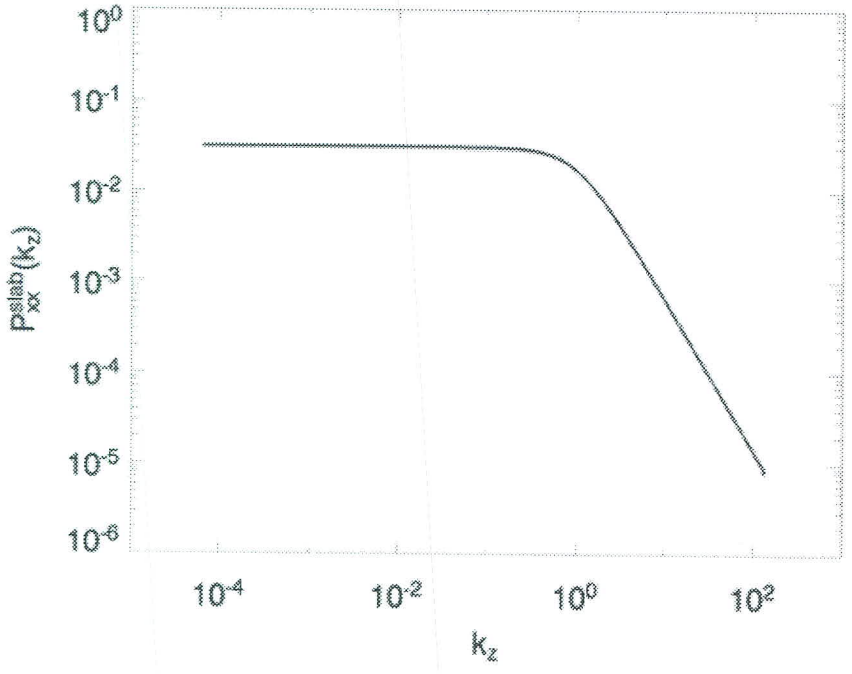

Figure 2.2 Example of a slab power spectrum.

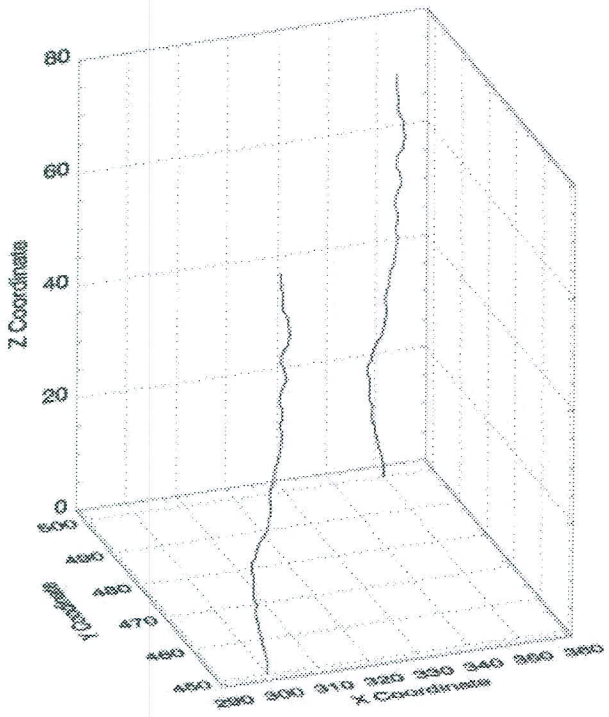

Figure 2.3 Example of two trajectories of magnetic field lines in pure slab turbulence.

2.1.2 Two Dimensional (2D) Fluctuations

For 2D field, the fluctuation depends only x and y coordinate. Since $\vec{\nabla} \cdot \vec{B} = 0$, we have $\vec{B} = \vec{\nabla} \times [a(x,y)\hat{z}]$, where $a(x,y)$ is the vector potential. In this work, we create 2D field in two cases. For the first case, the 2D field is turbulent. To generate this type of fluctuation, we need to specify power spectrum in wave number space. Another case is simple 2D field which model as only one single island. Here the potential function is simply defined by a Gaussian function.

I. Two dimensional (2D) Turbulence

From $\vec{B} = \vec{\nabla} \times [a(x,y)\hat{z}]$, we can write 2D turbulence as $\vec{b}_{2D} = \vec{\nabla}a(x,y) \times \hat{z}$. From this relation, we can clearly see that the 2D field must be in the direction perpendicular to the gradient of the potential function and also to the z direction. Therefore, the direction of the 2D field must be along the equipotential line of $a(x,y)$ as shown in Figure 2.4. A 2D field that has

a positive value of $a(x,y)$ is in a counterclockwise direction while one that has a negative value has a clockwise direction. When we consider the pure 2D turbulence $[B_0\hat{z} + \vec{b}_{2D}(z)]$, the field lines conserve the value of the potential function and move along the contour of $a(x,y)$. The example is shown as Figure 2.5.

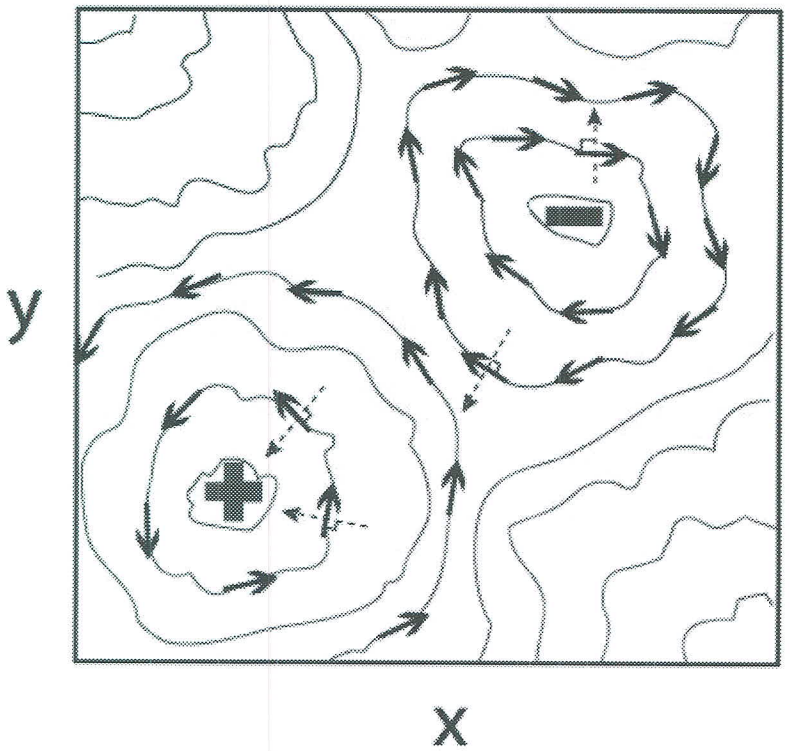

Figure 2.4 Schematic contour plot of $a(x,y)$. The solid arrows show the 2D field, $\vec{b}_{2D}$, and the dashed arrows show examples of the directions of $\vec{\nabla}a(x,y)$ for both positive and negative potential functions. The 2D field must lie along the equipotential lines of the potential function. For a positive potential function, the 2D field is in a counter-clockwise direction, while a 2D field having a negative potential function is in the clockwise direction.

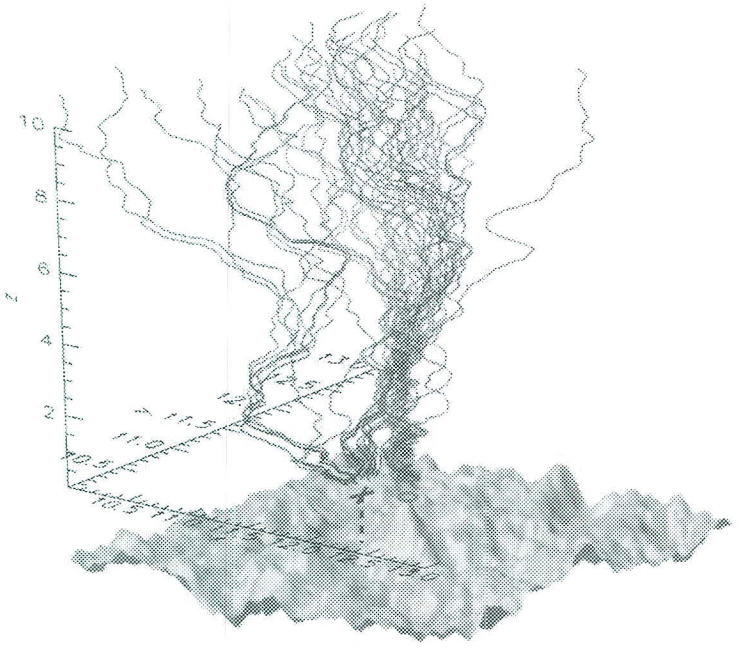

Figure 2.6 Sample of magnetic field lines in 2D+slab magnetic field turbulence that start at the difference locations. The field lines near O-point are trapped along some distance before they diffuse while the field line near X-point quickly spread at the beginning (Chuychai et al. 2007).

II. Simple Gaussian 2D Field

To understand the mechanism of separation between charged particles and their field lines, we also create a simple model for 2D field. For the simple case, we model 2D field as a Gaussian function while the slab field is turbulent (Chuychai et al. 2005; Tooprakai et al. 2007). That would provide us more understanding about the mechanism of the motion of the charged particles when we vary the initial pitch angles. The potential function for simple 2D case can be written as

$$a(r) = A_0 \exp\left[-\frac{r^2}{2\sigma^2}\right], \tag{2.3}$$

where A_0 is the central maximum value, σ determines the width of the Gaussian, and the distance r is measured from the axis of the flux tube. Without the slab field, the field line trajectories in this model, $B_0\hat{z} + \vec{b}_{2D}(x,y)$, have helical orbits along a cylindrical surface of constant $a(x,y)$ with a constant angular frequency as a function of z. The contour of $a(x,y)$ in this model is circle and field line move along the surface of constant $a(x,y)$ as shown in Figure

2.7. Then when we add slab turbulence, the example of trajectories are in Figure 2.8. The field lines start inside 2D island are trapped at the beginning and later become diffusive due to slab turbulence. For the field lines start outside, they quickly spread due to slab turbulence.

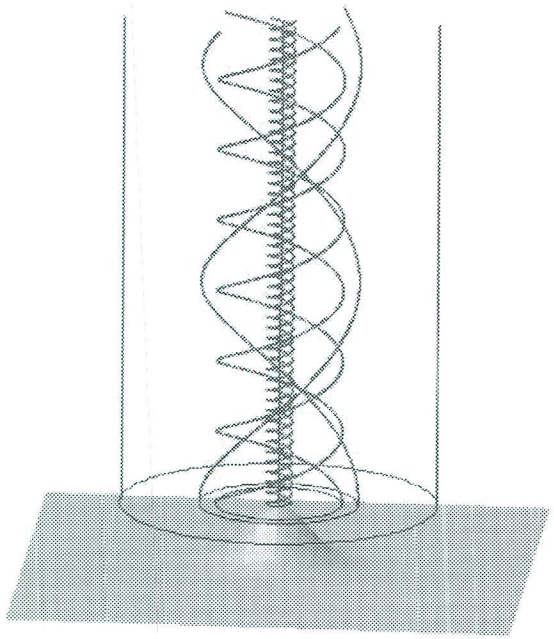

Figure 2.7 Magnetic field line trajectories for a single 2D island, with $\vec{B} = B_0\hat{z} + \vec{b}_{2D}(x, y)$. The surface plot at bottom shows the potential function $a(x, y)$ of the 2D field (Chuychai et al. 2007).

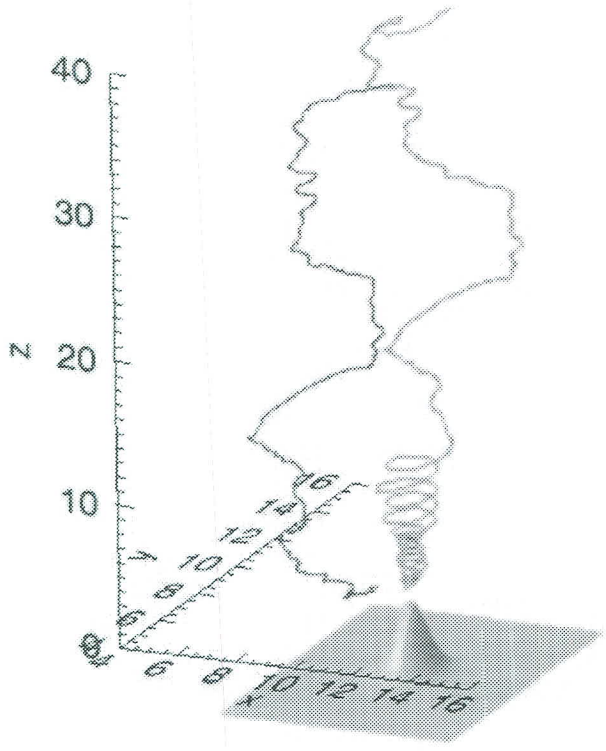

Figure 2.8 Example of two magnetic field lines in a single 2D Gaussian island plus slab turbulence. The red field line started deep inside the island, whereas the blue field line was initially located outside the island. The surface plot at bottom shows the potential function $a(x, y)$ of the 2D field (Chuychai et al. 2007).

2.2 Turbulent Magnetic Field with Taylor Microscale

In this section, we specify the magnetic field with microscale in order to develop the measuring technique and apply to spacecraft data (Chuychai et al. 2014). We use synthetic data generated using a known spectrum, and then employ a typical methodology to evaluate the Taylor microscale. The spectrum is constructed with inertial and dissipation ranges that have been independently controlled, and have generally different power law indices. To be specific, we let the inertial range have a spectral index of -5/3, while the dissipation range has an adjustable spectral index q. The particular functional form of the spectrum is

$$P(f) = \begin{cases} \frac{c}{[1+(f\tau_0)^2]^{\frac{5}{6}}}, \text{where } f_{min} < f \leq f_d \\ \frac{c}{[1+(f_d\tau_0)^2]^{\frac{5}{6}}}\left(\frac{f_d}{f}\right)^q, \text{where } f_d < f \leq f_e \\ 0, \text{ where } f_e < f \leq f_{max}, \end{cases} \quad (2.4)$$

where $q < 0$ (See the shape of spectrum is presented in Figure 3.1). The reasons for these choices are as follows: First, the flat spectral region at very low frequencies $f\tau_0 \ll 1$ is designed to make the signal time stationary. This is unrealistic for the solar wind, which has very low frequency components due to, eg, solar rotation and solar cycle (see e.g., Matthaeus and Goldstein 1982). However we are not concerned with very low frequency effects here. Second, the inertial range with Kolmogorov spectral index of ~5/3 is found for higher frequencies, at $f\tau_0 > 1$. Third, there is a discontinuous jump at the top of the inertial range at frequency f_d, the slope steepening from $-5/3$ to $-q$, in qualitative accord with observations (Leamon et al. 2008; Alexandrova et al. 2009; Sahraoui et al. 2009). Finally at high frequencies $f > f_e$ we set the spectrum to zero, for numerical rather than physical reasons, to provide a very smooth trigonometric interpolation of the signal at the grid scale.

Adopting illustrative values that are representative of the solar wind at 1AU, we assume that the spectrum starts from $f_{min} = 1.22 \times 10^{-5}$ Hz and is flat until $f_0 = \frac{1}{\tau_0} = 3.906 \times 10^{-4}$ Hz, a "bendover" frequency often associated with the correlation scale or coherence time. Thereafter the spectrum has an inertial range with a 5/3 power law index, until a second break point is encountered at $f_d = 1/\tau_d = 0.4$ Hz. For historical reasons, this breakpoint, which terminates the power law MHD-scale inertial range, is often referred to as the "dissipation scale" (Leamon et al. 1998), although it is also possible that it characterizes dispersion rather than dissipation (Gary and Borovsky 2004). In the hydrodynamic case for which the eddy turnover time and viscous dissipation time scales become equal at the dissipation scale, for the solar wind or other low-collisionality astrophysical plasmas, it is unclear whether the fluctuations become critically damped at the breakpoint/dissipation scale. For example, the inertial range is typically found to terminate near the proton gyroscales, and while some dissipation may occur at such scales, further kinetic plasma dynamics may transfer energy to higher frequencies until much smaller electron scales are encountered (Alexandrova et al. 2009; Sarhaoui et al. 2009). It has been argued that a substantial fraction of actual dissipation may occur due to electrons. In any

case the scale f_d corresponds to the onset of kinetic processes and the end of the Kolmogoroff-like inertial range. It is, however, the kinematic properties of the spectrum that come into play in the current study, rather than the dynamical origin of the spectral forms.

In our model development, beyond the breakpoint f_d, we extend the dissipation range with power law index q until f_e = 16.0 Hz which may be considered, in the solar wind application, to be associated with the electron dissipation scale. The spectrum cuts off completely at f_{max}=25.6 Hz. To decide upon these numerical values, here we assume that the dissipation scale and electron dissipation scale correspond to the proton and electron inertial scales, respectively. Thus we set $\frac{f_e}{f_d} = 40$ to be consistent with the ratio of electron and proton inertial scales in MHD, which is about $\sqrt{m_p/m_e} = 42.9$ (see e.g., Sahraoui et al. 2009).